# REPORT DOCUMENTATION PAGE

Form Approved
OMB NO. 0704-0188

| 1. AGENCY USE ONLY (Leave Blank) | 2. REPORT DATE **October 31, 2001** | 3. REPORT TYPE AND DATES COVERED **Final Report May 2001 – October 2001** |
|---|---|---|

**4. TITLE AND SUBTITLE**

**UV/Blue III-Nitride Micro-Cavity Photonic Devices (In response to SBIR topic N01-045)**

**5. FUNDING NUMBERS**

**N00014-01-M-0111**

**6. AUTHOR(S)**

**Hongxing Jiang and Jingyu Lin**

**7. PERFORMING ORGANIZATION NAME(S) AND ADDRESS(ES)**
**III-N Technology, Inc.**
**2033 Plymouth Road**
**Manhattan, KS 66503**

**8. PERFORMING ORGANIZATION REPORT NUMBER**

**N00014-01-M-0111- 0001AA**

**9.SPONSORING / MONITORING AGENCY NAME(S) AND ADDRESS(ES)**
**Office of Navel Research**
**Attn: Dr. Yoon Soo Park**
**Ballston Tower One**
**800 North Quincy Street**
**Arlington, VA 22217-5660**

**10. SPONSORING / MONITORING AGENCY REPORT NUMBER**

**11. SUPPLEMENTARY NOTES**
    **The views, opinions and/or findings contained in this report are those of the author(s) and should not be construed as an official Department of the Navy position, policy or decision, unless so designated by other documentation.**

| 12 A. DISTRIBUTION / AVAILABILITY STATEMENT **Approved for public release; distribution unlimited.** | 12 B. DISTRIBUTION CODE |
|---|---|

**13. ABSTRACT (Maximum 200 words)**
Consistent with our tasks, we have further improved our micro-size light emitter output efficiencies by optimizing device layer structures, including superlattice structures for enhancing the hole concentration, the thickness of the top Mg doped p-type layer to reduce the light absorption, and the structure of the active region. We have also carried out measurements on the size dependence of the micro-size light emitter characteristics. It was found that the micro-LEDs were very efficient and the heating effect was not significant in micro-LEDs that are greater than 10 $\mu$m in diameter. Our results also revealed that the operating speed increases with decreasing micro-LED size and the response time reduced from 0.21 ns for 15-$\mu$m LEDs to 0.15 ns for 8-$\mu$m LEDs. Several integrated photonics devices have been fabricated and their operation under current injection has been achieved. Sub-micron waveguides have also been fabricated from AlGaN/GaN multiple quantum wells and their optical properties have been measured. Effects related to reduced size have been observed. The ability of 2D array integration with advantages of high speed, high resolution, low-temperature sensitivity, and applicability under versatile conditions, make III-nitride micro-photonics unique for many applications, such as optical communications, chemical- and bio-agents detection.

| 14. SUBJECT TERMS UV/blue Optoelectronics and Photonics, Microcavity LEDs, Microcavity Lasers, III-Nitride Wide Bandgap Semiconductors, Lighting | 15. NUMBER OF PAGES 7 |
|---|---|
| | 16. PRICE CODE |

| 17. SECURITY CLASSIFICATION OR REPORT **UNCLASSIFIED** | 18. SECURITY CLASSIFICATION ON THIS PAGE **UNCLASSIFIED** | 19. SECURITY CLASSIFICATION OF ABSTRACT **UNCLASSIFIED** | 20. LIMITATION OF ABSTRACT **UL** |
|---|---|---|---|

Standard Form 298 (Rev.2-89)
Prescribed by ANSI Std. 239-18
298-102

20011105 043

**Project Title:** UV/Blue III-Nitride Micro-Cavity Photonic Devices
**Topic Number:** N01-045
**Principal Investigator:** Hongxing Jiang
**Firm Name:** III-N Technology, Inc.
**Authors:** Hongxing Jiang
Jingyu Lin
**Address:** 2033 Plymouth Road, Manhattan, KS 66503
**Publication Date:** October 31, 2001
**Contract Number:** N00014-01-M-0111
**Period Covered:** May 2001 - Oct. 2001

The main objectives of this Phase I research are to
- Further develop III-nitride microcavity photonic device technologies;
- Demonstrate the feasibility of achieving electrically pumped III-nitride microcavity emitter;
- Assess the feasibility of integrating miniaturized light emitter arrays with waveguides.

The objectives are to be accomplished through the work plan that can be divided into five tasks, which are summarized in Table I.

### Table I. Proposed Task Schedule Based on the Month After Receipt of Phase I Award

| Tasks | Time, Months | | | | | | | | |
|---|---|---|---|---|---|---|---|---|---|
| | Phase I Duration | | | | | | Optional Duration | | |
| | 1 | 2 | 3 | 4 | 5 | 6 | 7 | 8 | 9 |
| **1. Optimizing μ-cavity emitter materials & structures**<br>• Blue μ-cavity photonic materials & device structures<br>• UV μ-cavity photonic materials & device structures | | ☐ | ☐ | ☐ | ☐ | ☐<br>☐ | ☐<br>☐ | ☐ | |
| **2. Optimizing μ-cavity emitter fabrication processes**<br>• Patterning by lithography and ICP dry etching<br>• Self-organization by selective area overgrowth | | ☐ | ☐ | ☐ | ☐ | ☐<br>☐ | ☐<br>☐ | ☐ | |
| **3. Characterization of individual μ-light emitters**<br>• I-V, L-I, E-L characteristics vs. μ-cavity lateral size;<br>• Polarization and directionality dependence of the lasing spectra;<br>• Turn-on and off speed vs. μ-cavity lateral size;<br>• Operating lifetimes under pulsed and cw injections. | ☐ | ☐ | ☐ | ☐ | ☐ | ☐ | ☐ | | |
| **4. Coupling between μ-emitter arrays with waveguides** | | | | | | | ☐ | ☐ | ☐ |
| **5. Final Report** | | | | | | | | | ☐ |

Consistent with our tasks, we have carried out the following studies:

1. <u>Further improving blue microcavity photonics device structures.</u>

We have investigated methods for further enhancing the emission efficiency of InGaN/GaN LEDs. The new LED wafers were grown on sapphire substrates with 30 nm GaN buffer layers by low pressure MOCVD. The device structure includes a 3.5 μm of silicon doped GaN, 10 periods of Si doped superlattice consisting of alternating layers of AlGaN (30 Å)/GaN (30 Å), a 0.05 μm of Si doped GaN, two periods of InGaN (30 Å)/GaN (25 Å) undoped quantum well active region. Followed by 14 periods of Mg doped superlattice consisting of alternating layers of AlGaN (30 Å)/GaN (30 Å), and 0.1 μm Mg-doped GaN epilayer. The structure was then thermally annealed at 950 °C for 8 seconds in nitrogen in a rapid thermal-annealing furnace to activate Mg acceptors. By incorporating the modified superlattice structure into the device and decreasing the top Mg-doped p-type layer thickness to 0.1 μm, we have enhanced the power output of our conventional broad area (300 x 300 μm$^2$) purple LEDs (408 nm) by a factor of 2. Further improvements in materials and structural qualities are needed in order to fabricate microcavity lasers based on these materials.

2. <u>Characterization of micro-size light emitters</u>
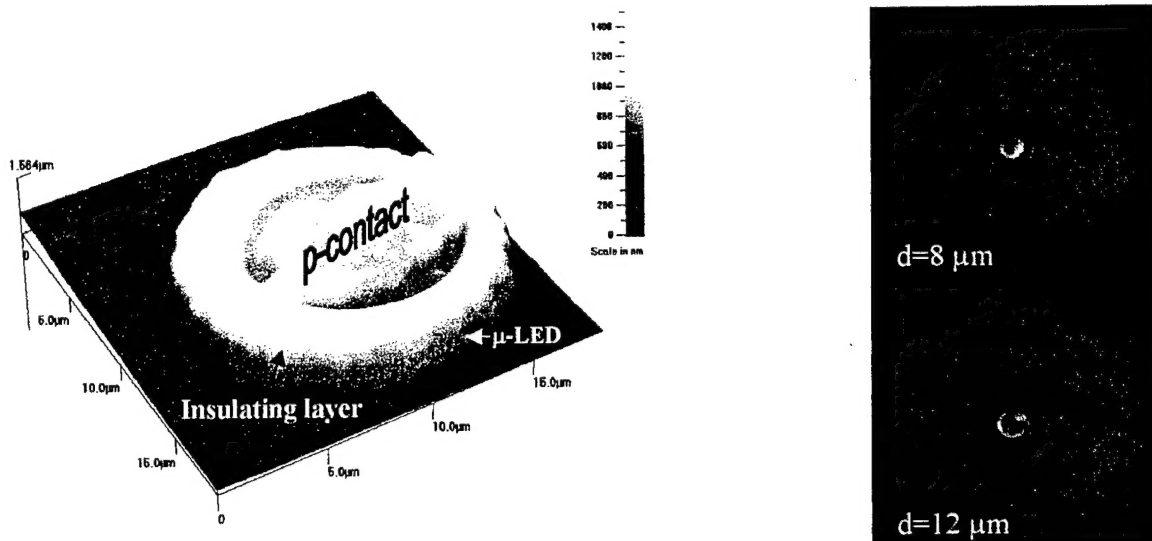
# III-Nitride Blue Micro-LEDs



Fig. 1 (a) An AFM image showing a fabricated micro-LED. (b) Optical microscope images of individual μ-disk LEDs in action.

Dring the reporting period, individual μ-disk LEDs of varying diameters from 5 to 20 μm were fabricated by photolithography patterning and inductively coupled plasma (ICP) dry etching. Bilayers of Ni (20nm)/Au (200nm) and Al (300nm)/Ti (20nm) were deposited by electron beam evaporation as p- and n-type Ohmic contacts. The p-type contacts and the n-type contacts were thermally annealed in nitrogen ambient at 650 $^0$C for 5 min. A dielectric layer was deposited by e-beam evaporation after the μ-LEDs formation for the purpose of isolating p-type

contacts from the etch-exposed n-type layer. This allowed us to carry out preliminary measurements on the size dependence of the μ-LED characteristics. Figure 1 (a) shows an atomic force microscope (AFM) image of a fabricated μ-LED. As can be seen from Fig. 1(a), the p-type contact was connected to the top p-layer by opening a hole through the insulating dielectric layer. The size of the p-type contact is about 4 μm in diameter. Figure 1(b) shows optical microscope images, taking from the top (p-type contact side), of two representative InGaN/GaN QW μ-LEDs with diameters d=8 and 12 μm in action with an injected current of 2 mA. The p-type contacts on the top layers are also visible in Fig. 1(b).

The I-V characteristics of μ-disk LEDs of varying sizes and a conventional board-area LED (300 x 300 μm$^2$) fabricated from the same wafer are plotted in Fig. 2 (a) linear and (b) semi-logarithmic scales. It is clearly seen that the turn-on voltages for individual μ-LEDs are larger than that of the broad-area LED. Among the μ-LEDs of different sizes, the turn-on voltage increases with decreasing μ-LED size. The slope of the Log I vs. V plot in Fig. 2(b) reflects the ideality factor, n (=1/slope). It is clear that the ideality factor of μ-LEDs (n=18.5) is larger than that of the broad-area LED (n=6.4). There is only a weak size dependence of ideality factor for the μ-disk LEDs. The larger ideality factor reflects the enhanced non-radiative recombination in μ-LEDs, which is most likely a result of enhanced surface recombination around the edge of the disk of μ-LEDs.
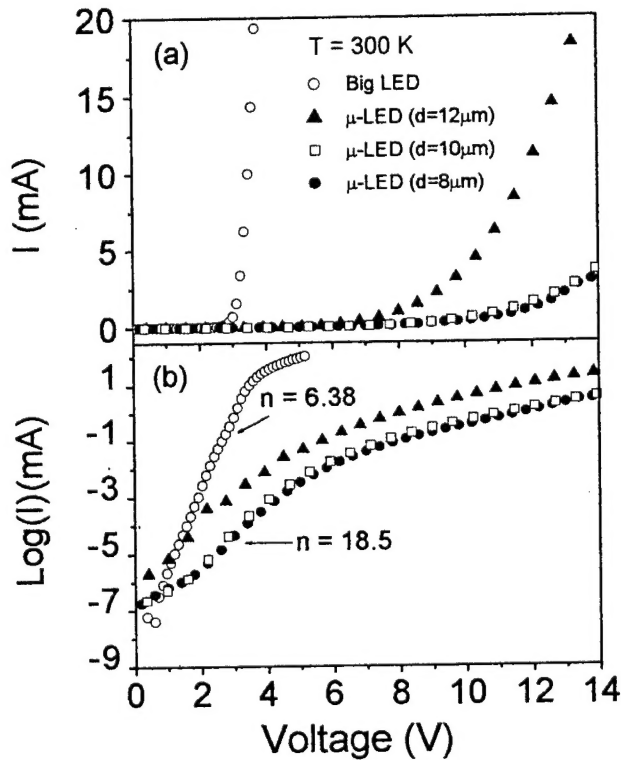


Figure 2 I-V characteristics of μ-LEDs of varying sizes (d =8, 10, and 12 μm) and a broad-area LED (300 x 300 μm$^2$) in (a) linear and (b) semi-logarithmic plots.
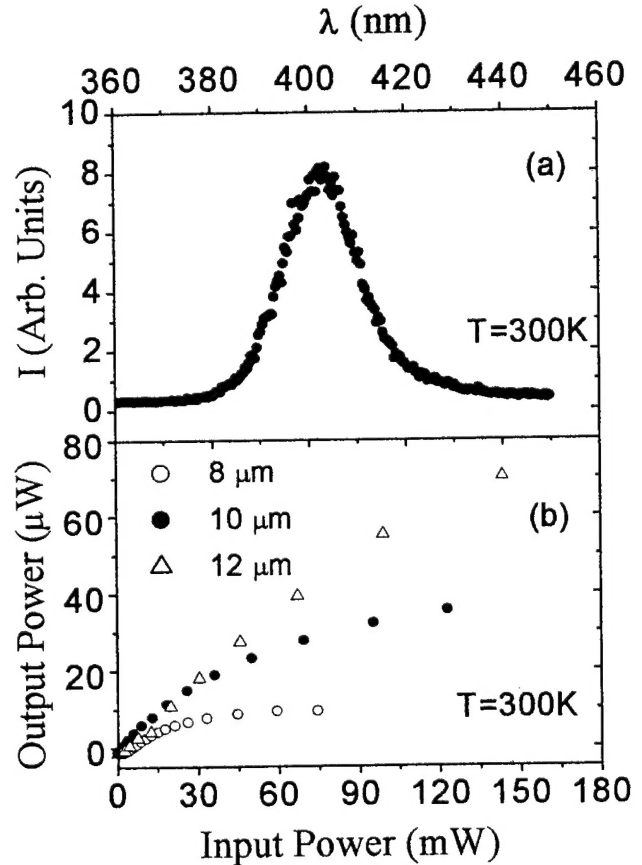


Figure 3 (a) E-L emission spectrum of a purple μ-LED. (b) Output power vs. input power (L-I) plot of μ-LEDs of different sizes.

Figure 3 shows a room temperature electro-luminescence (EL) spectrum of a purple μ-LED measured at a forward current of 2 mA. Fig. 3(b) plots the output power vs. input power measured from the sapphire substrate side for three unpackaged μ-LEDs of different sizes. Heating effects become more prominent as the size of μ-LEDs decreases. For μ-LEDs with d=12 μm, the output power increases almost linearly with input power in the entire measured range. However, for μ-LEDs with d=8 μm, the output power saturates at about 10 μW for input power above about 45 mW. As expected, heat dissipation is more difficult in μ-LEDs with reduced sizes, which causes power output saturation. However, we believe that appropriate packaging processes can improve the performance.

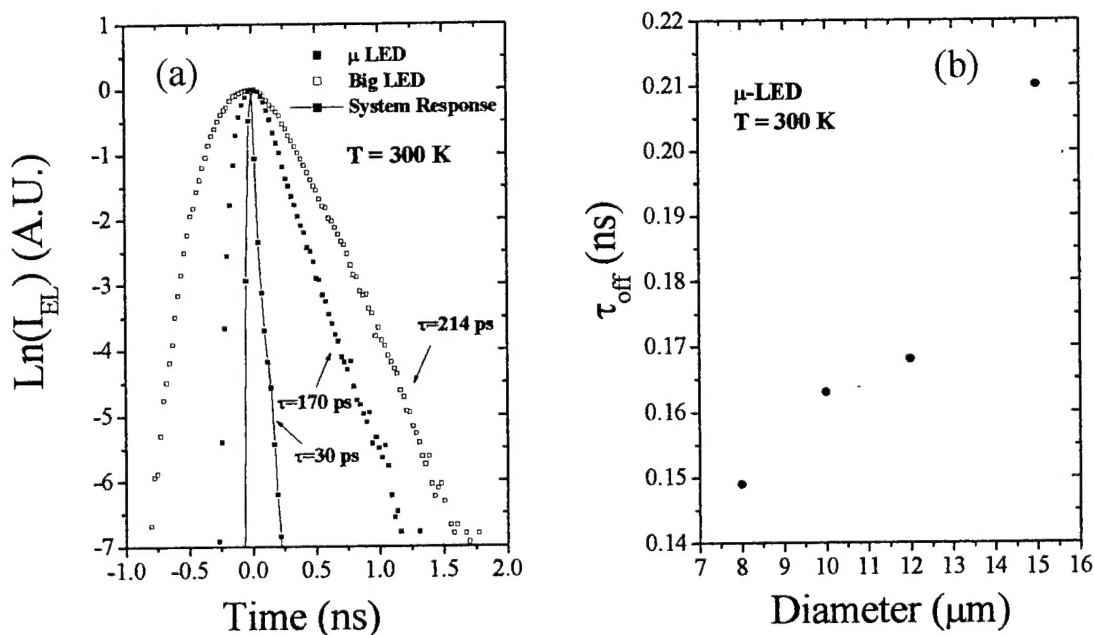## Transient Responses of III-nitride μ-LEDs



Fig. 4 (a) Transient responses of a microdisk LED of 12 μm in diameter and a broad-area LED (300 x 300 μm2) in response to picosecond electrical pulses. The turn on time of the microdisk LEDs is on the order of the system response ( < 35 ps). (b) The size dependence of the turn-off time of the microdisk LEDs. $\tau_{off}$ decreases with a decrease of μ-LED size. It reduced from 0.21 ns for d=15 um to 0.15 ns for d=8 um.

These μ-LEDs have potential applications in short distance optical communications. For these applications, the speed is one of the most crucial parameters, which has been measured by time-resolved EL. In Fig. 4 we plotted (a) transient responses of a μ-LED and a conventional broad-area LED and (b) the size dependence of the "turn-off" time, $\tau_{off}$, of μ-LEDs. The turn-on response was very fast and could not be measured. However, the turn-off transient was in a form of single exponential and its lifetime, $\tau_{off}$, could be determined. It was found that $\tau_{off}$ decreases with a decrease of μ-LED size. It reduced from 0.21 ns for d=15 μm to 0.15 ns for d=8 μm. This behavior is also expected since the effects of surface recombination are enhanced in smaller μ-LEDs. On the other hand, the increased operating speed may also be a result of an enhanced radiative recombination rate in μ-LEDs. With this fast speed and other advantages such as long

4

operation lifetime, III-nitride μ-LED arrays may be used to replace lasers as inexpensive short distance optical links such as between computer boards with a frequency up to 10 GHz.

### 3. Fabrication and characterization of novel μ-light emitter structures

#### a) III-nitride sub-micron waveguides

We have also successfully fabricated submicron waveguide structures based on AlGaN/GaN multiple-quantum wells (MQW). The waveguides are important component in integrated photonic circuits. The waveguides were patterned with widths varying from 0.5 – 2.0 μm and orientations varying from -30° to 60° relative to the a-axis of GaN. Fig. 5 (top) shows the SEM images of two sets of waveguides. We found that when the width of waveguides was reduced to below 0.7 μm, as illustrated in Fig. 5 (bottom), the emission peak position and line-width of the localized exciton emission were found to vary systematically with orientations of the waveguides and followed the six-fold symmetry of wurtzite structure. This is related to the anisotropy of the exciton/carrier diffusion coefficient along the different crystal orientations in quasi one-dimensional case.
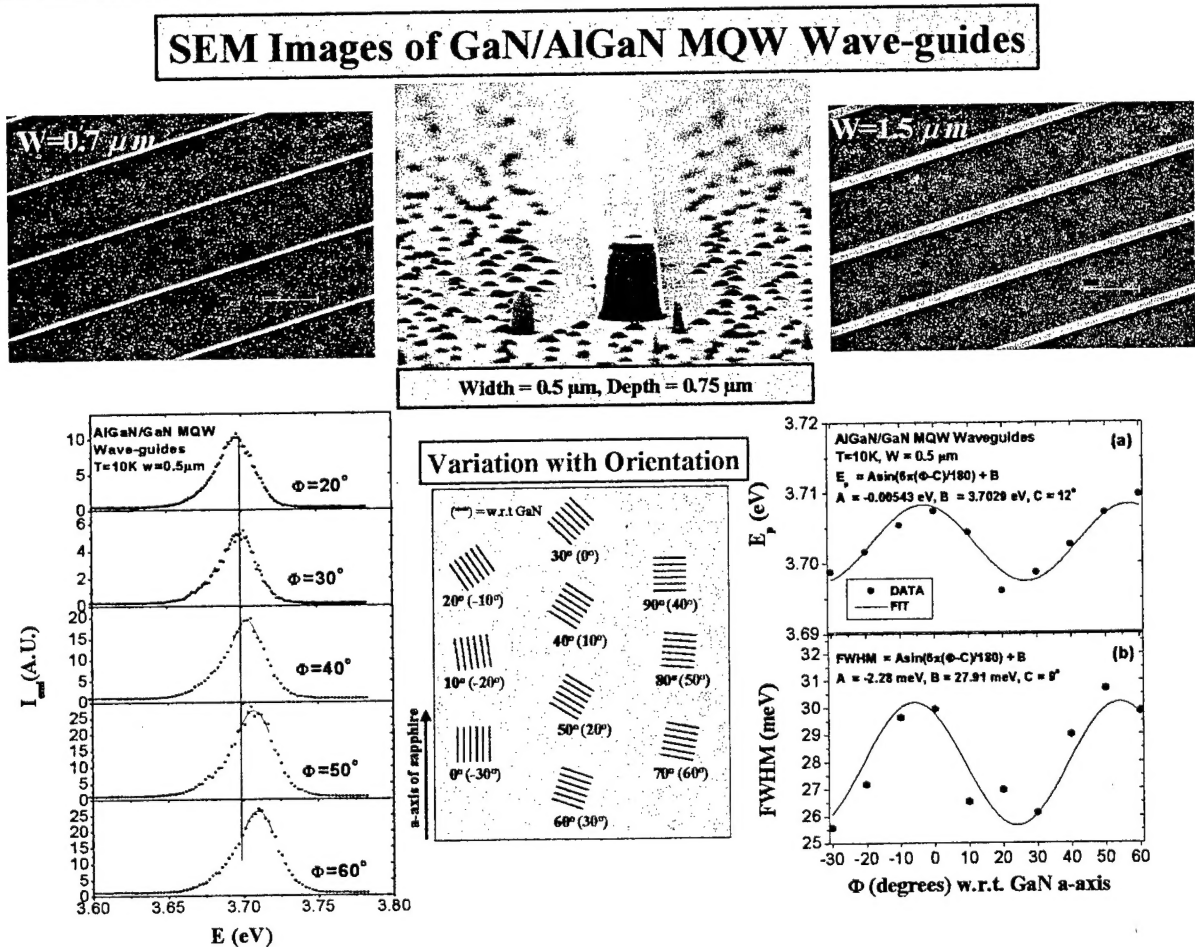


Fig. 5 (Top) SEM images of AlGaN/GaN MQW waveguides. (Bottom: left) Low temperature (10 K) cw PL spectra from AlGaN/GaN MQW waveguides of different line orientations; (Bottom: right) the variation of (a) the spectral peak positions ($E_p$) and (b) full width at half maximum (FWHM) of the PL emission line at 10 K. The solid line is the sinusoidal fit of the data with 6-fold symmetry of hexagonal structure. (Center) Schematic of a set of AlGaN/GaN QW waveguides with varying orientation.

By analyzing the arrangements of $Ga^{3+}$ and $N^{3-}$ ions in a hexagonal GaN crystal, it was clear that the crystal arrangements along the directions parallel to $0°/60°$ and $-30°/30°$ are different. The a-axis of GaN is shifted $30°$ with respect to the a-axis of sapphire. Waveguides prepared along $-30°/30°$ (where $E_p$ and FWHM are minimum) and $0°/60°$ (where $E_p$ and FWHM are maximum) have the following differences in crystal arrangements:

1. The number of ions per unit length in the $-30°/30°$ line is greater than that along the $0°/60°$ line by a factor of 10:9.
2. The lateral termination of the waveguides for the $-30°/30°$ line is composed of both Ga and N ions while that of the $0°/60°$ line is either Ga or N.
3. The width covered by 4 columns of ions is larger in the $-30°/30°$ direction than in the $0°/60°$ direction.

These differences could be the source of the anisotropy of the exciton/carrier diffusion coefficient in the quasi-1D waveguide structures. At $0°/60°$ orientations, there is slow carrier or exciton diffusion leading to band-filling effect with the result that $E_p$ and FWHM are both maximum. Faster diffusion occurs along the $-30°/30°$ resulting in $E_p$ and FWHM both being minimum. Our results indicate that there is a difference in optical property of submicron structures, shown by the periodic variation in the peak energy $E_p$ and FWHM of the spectra from MQW waveguides at different crystal orientations. This difference is more pronounced in smaller structures.

Our results imply that in photonic structures with submicron sizes are involved, there will be differences in exciton or carrier dynamics. The differences arising from the choice of orientation will result in significant effects in the associated devices. Such devices include optical waveguides, photodetectors and ridge wave guide laser diodes. Therefore in the design of these devices, proper attention must be paid in the choice of the orientation of the associated submicron structures.
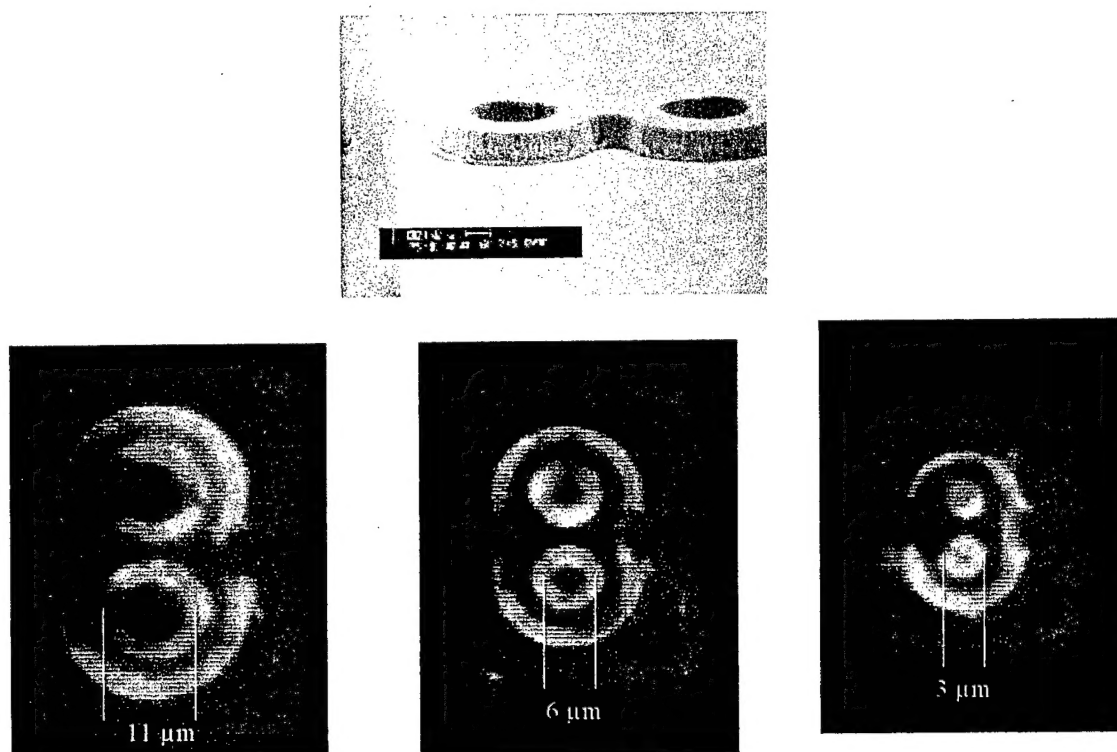
## b) *Double-ring micro-cavity light emitters*

We have succeeded in fabricating double-ring μ-cavity light emitters. We have obtained a bonding scheme (as shown in Fig. 6) that will allow the detailed characterization of these novel light emitters under different current injection conditions. As illustrated in Fig. 7, their operation under current injection has been achieved. The current-voltage (I-V) and output power-current (L-I) characteristics have been measured and the results for three double-ring micro-cavity light emitters of different sizes are shown in Fig. 8. Comparing with microdisk LED I-V characteristics shown in Fig. 2(a), the turn on voltage is almost independent of size for double-ring cavity emitters.

It is also interesting to note that, the L-I characteristics of bare microdisk LEDs shown in Fig. 3(b) indicates that the power output saturated around 10 and 40 μW at 30 and 100 mW input power for disks of 8 and 10 μm, respectively possibly due to the fact that the heating effect becomes more prominent in smaller size microdisk LEDs. Whereas the power output increases linearly with input power and no saturation occurs even in the bare double-ring emitter of the smallest size (inner-ring 3 μm and out-ring 15 μm). Furthermore, the power output remains almost the same for the three emitters of different sizes, which indicates that the efficiency per unit area is significantly enhanced in the double-ring emitters of reduced size. Our results have clearly shown the advantages of the double-ring light emitter structures, as they could handle

# III-Nitride Double-Ring μ-Cavity Light Emitters



**Fig. 6** Optical microscope image of a fabricated III-nitride double-ring microcavity emitter with n- and p-contact pads, which can be used for current injection and charaterization.

# III-Nitride Double-Ring μ-Cavity Light Emitters



**Fig. 7** Top: Scanning electron microscopy (SEM) image of a double-ring microcavity emitter prior to electrical contacts fabrication. Bottom: Optical microscope images of III-nitride double-ring microcavity emitters of different sizes in operation.

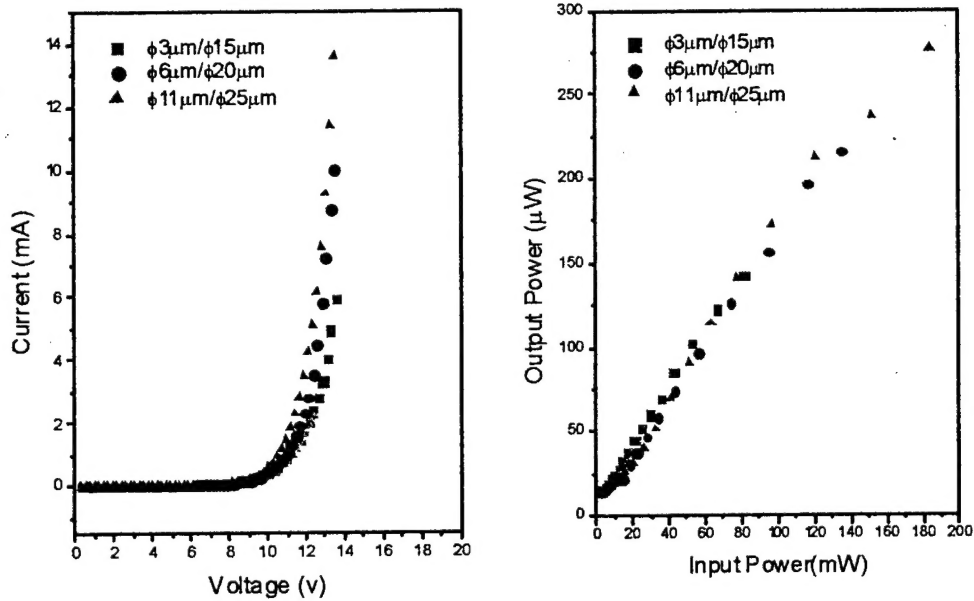## I-V and L-I Characteristics of Double-Ring Micro-Size Emitters



Fig. 8 Current-voltage (I-V) characteristics (left) and output power vs. input power (right) of bare double-ring microcavity light emitters.

more heat and at the same time delivering higher power efficiency. Further work is needed in order to obtain real practical micro-size devices from these unique structures.
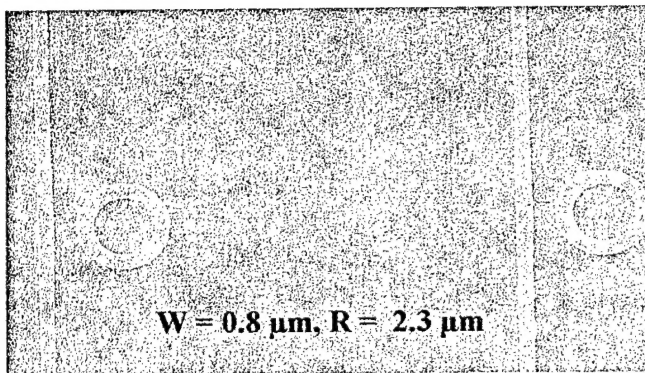
### c) *Integrated microstructures*



Fig. 9 SEM images of integrated photonic structures consisting of sub-micron waveguides and resnonators.

We have also fabricated integrated microstructures consisting of wave-guides and resonators [Fig. 9]. With strong lateral confinement, wavelength-scale waveguides and disk or the ring cavity resonators can have very small sizes with negligible bending loss. They can provide very high-density optical circuitry. For the ring (disk) resonator, if the mode supported by the adjacent waveguide matches the whispering-gallery-mode (WGM) propagating in the ring (disk), it will support single-mode behavior within the disk and optimize disk-to-waveguide coupling. A combination of these elements can build intelligent devices for many applications.

We intend to characterize these photonic components in detail. We also intend to further develop in phased II the micro- and nano-fabrication technologies and new architectures for integrating different photonic components onto single chips for a variety of applications, such as optical communications, chemical- and bio-agents detection.